

A Unified Fitting of H I and He II Ly α Transmitted Flux of QSO HE2347 with Λ CDM Hydrodynamic Simulations

Jiren Liu¹, Priya Jamkhedkar², Wei Zheng³, Long-Long Feng^{4,5}, and Li-Zhi Fang²

ABSTRACT

Using cosmological hydrodynamic simulations of the LCDM model, we present a comparison between the simulation sample and real data sample of H I and He II Ly α transmitted flux in the absorption spectra of the QSO HE2347-4342. The Λ CDM model is successful in simultaneously explaining the statistical features of both H I and He II Ly α transmitted flux. It includes: 1.) the power spectra of the transmitted flux of H I and He II can be well fitted on all scales $\geq 0.28 \text{ h}^{-1} \text{ Mpc}$ for H, and $\geq 1.1 \text{ h}^{-1} \text{ Mpc}$ for He; 2.) the Doppler parameters of absorption features of He II and H I are found to be turbulent-broadening; 3.) the ratio of He II to H I optical depths are substantially scattered, due to the significant effect of noise. A large part of the η -scatter is due to the noise in the He II flux. However, the real data contain more low- η events than simulation sample. This discrepancy may indicate that the mechanism leading extra fluctuations upon the simulation data, such as a fluctuating UV radiation background, is needed. Yet, models of these extra fluctuations should satisfy the constraints: 1.) if the fluctuations are Gaussian, they should be limited by the power spectra of observed H I and He II flux; 2.) if the fluctuations are non-Gaussian, they should be limited by the observed non-Gaussian features of the H I and He II flux.

Subject headings: cosmology: theory - large-scale structure of the universe

¹Center for Astrophysics, University of Science and Technology of China, Hefei, Anhui 230026, P.R.China

²Department of Physics, University of Arizona, Tucson, AZ 85721

³Department of Physics and Astronomy, Johns Hopkins University, MD 21218

⁴Purple Mountain Observatory, Nanjing, 210008, P.R. China.

⁵National Astronomical Observatories, Chinese Academy of Science, Chao-Yang District, Beijing 100012, P.R. China

1. Introduction

$\text{Ly}\alpha$ forest lines and transmitted flux of QSOs' absorption spectra provide the most valuable samples in studying the physical state of the intergalactic medium (IGM) and gravitational clustering at high redshifts. High resolution samples of QSOs' $\text{Ly}\alpha$ absorption spectra are important to test models of cosmic structure formation on small scales. Recently, the H I $\text{Ly}\alpha$ transmitted flux of HE2347-4342 has been used to compare with hydrodynamical simulation samples of the ΛCDM model (Jamkhedkar et al. 2005, here after Paper I). The results suggest that the ΛCDM model is successful in explaining the power spectrum and intermittency of the HE2347-4342 sample. There is no discrepancy between the simulated and observed flux fields with regards to their statistical behavior from the second to the eighth orders and till the comoving scales as small as about $0.28 \text{ h}^{-1} \text{ Mpc}$. This result seems not to support the necessity of reducing the power of density perturbations relative to the standard ΛCDM model on small scales, as was implied by the lack of dense cores in the halo's center given by the so-called universal density profile (Flores & Primack 1994; Swaters et al. 2003; McGaugh et al. 2003; Zentner & Bullock 2003; Simon et al. 2003)

The IGM is also traced by He II $\text{Ly}\alpha$ absorption. Because the ionizing threshold of He II is high (54.4 eV), and recombination rate of He III is also high, the He II $\text{Ly}\alpha$ absorption of IGM generally is much stronger than H I $\text{Ly}\alpha$. Therefore, it is expected that the He II $\text{Ly}\alpha$ forest and transmitted flux of high redshift QSOs can play a similar role as H I forests in constraining cosmological models, and can even yield stronger constraints on the models than H I forests (Zhang et al. 1995; Croft et al. 1997). However, due to the lack of He II data, the comparison of He II spectra between model predictions and observations could not be made in a similar way as for H I $\text{Ly}\alpha$ absorption spectra. Thanks to the *FUSE* data of HE2347-4342, we can obtain moderate resolution spectra of He II $\text{Ly}\alpha$ transmitted flux in the redshift range $2.0 < z < 2.9$ (Kriss et al. 2001). It provides the possibility of making a similar analysis as for the H I transmitted flux.

We cannot simply repeat the analysis as Paper I, because of a new problem: the ratio between the optical depths of He II and H I, $\eta = 4\tau_{\text{HeII}}/\tau_{\text{HI}}$. If assuming 1.) the effect of thermal broadening and peculiar velocities of IGM are negligible, and 2.) He II and H I are in photoionization equilibrium, the ratio η should basically be constant, and have a low level of scatter because η is weakly dependent on the temperature of IGM. Observations reveal, however, that η is significantly scattered from pixel to pixel, or from line to line (Kriss et al. 2001; Smette et al. 2002). For the *FUSE* data of HE2347-4342, the scatter of η is from 1 to a few hundreds (Shull et al. 2004), and even as high as $\simeq 10^4$ (Zheng et al. 2004).

The large η -scatter has been used as an indicator of the inhomogeneity of UV radiation background caused by the radiation transfer (RT) of the UV photons in a nonuniform density

field. A 3-dimensional radiation transfer calculation on the shadowing, self-shielding and filtering predicted that the mean of η should be as large as $\langle\eta\rangle > 200$ (Maselli & Ferrara 2005). However, the observed result is $\langle\eta\rangle < 100$ (Zheng et al. 2004; Shull et al. 2004). Therefore, the RT effect explanation of η scatter is far from settling. This result motivated us to reconsider the assumptions above mentioned. If above-mentioned assumptions 1.) and 2.) are not hold, the η -scatter would not be a direct measurement of the inhomogeneity of UV background.

In this paper, we will study the effect of thermal broadening and peculiar velocities on the H I and He II Ly α transmitted flux. It has been shown recently that in nonlinear regime the velocity field $v(x)$ of cosmic baryon matter consists of strong shocks on various spatial scales and in high and low mass density area (Kim et al. 2005). The statistical behavior of the velocity field is similar to a fully developed turbulence (He et al. 2006). Therefore, the effect of thermal broadening and peculiar velocities of IGM would not be negligible. We should, at least, estimate the imprints of the non-trivial velocity field on the Ly α forests of He II and H I.

The paper is organized as follows. Section 2 describes the observed data of HE2347-4342. Section 3 presents the method to simulate the Ly α forests of He II and H I. As in Paper I, we use the WIGEON method of cosmological hydrodynamic simulations to produce the simulation samples, as this code is especially effective in capturing singular and complex structures (Feng et al. 2004). On the other hand, He II would be formed in hotter gas, such as shock heated IGM (Cen & Ostriker 1999; Davé et al. 2001), a method of effectively simulating shocks would be important. Velocity field effect on absorption width is shown in Section 4. Section 5 presents the analysis of the ratio between the optical depths of He II and H I Ly α transmissions. The power spectrum of the H I and He II flux will be discussed in §6. Discussions and conclusions are given in §7.

2. Data of HE2347-4342

The data of H I Ly α transmitted flux used in this paper is the same as in Paper I. The *FUSE* data of the He II Ly α transmitted flux of HE2347-4342 is described in Zheng et al. (2004). The wavelength region is 904 – 1188 Å, which corresponds to the redshift range $2.0 \leq z \leq 2.9$, as the wavelength 303.78 Å of He II Ly α in rest frame. The spectrum has a constant bin size of $\Delta\lambda = 0.025$ Å. In terms of the local velocity, the resolution is $dv \simeq 8.3 - 6.3$ km s $^{-1}$, and mean $dv \simeq 7$ km s $^{-1}$. The mean S/N is 2.14. Following the approach of Shull et al. (2004), we bin the data into $\Delta\lambda = 0.05$ Å to reduce uncertainties in the effective spectrograph resolution and oversampling effect. The distance between N

pixels in the units of the local velocity scale is given by $\delta v = 2c[1 - \exp(-Ndv/2c)] \text{ km s}^{-1}$, corresponding to comoving scale $D = \delta v(1 + z)/H(z)$.

The flux in 2729 pixels, i.e., 24% of the total pixels, are less than zero. Obviously, the points with negative flux is unphysical, it should be excluded in the statistics below. For sample deleting all the pixels with negative flux, the mean transmission about 0.4, or effective optical depth ~ 0.9 . The optical depths of He II over the ranges from 0.1 to 2.3 are with 10% uncertainties. A better statistical measurement of the fluctuations of flux is given by the ratio between the optical depths of He II, τ_{HeII} , and H I, τ_{HI} , for each pixel. The distribution of η is scattered in the range from 0.1 to about 500, while the mean of η is $\simeq 80$ (Shull et al. 2004).

We also assume that all absorption in the *FUSE* spectrum is due to He II, although it is subject to metal-line contaminations. Generally identified metal-lines are connected with a Lyman-limit system (Smette et al. 2002). The Doppler width of metal lines are generally narrow with $\delta v \leq 20 \text{ km s}^{-1}$. In this paper, we restrict our analysis only to scales $\delta v \geq 30 \text{ km s}^{-1}$ where metal-line contaminations is low (Hu et al. 1995; Boksenberg et al. 2003; Kim et al. 2004).

3. Hydrodynamic simulation sample

3.1. Method

We use the cosmological hydrodynamic simulation samples produced by the Weno for Intergalactic medium and Galaxy Evolution and formatiON (WIGEON) code developed by Feng et al. (2004). It is a hybrid hydrodynamic/ N -body simulation, consisting of the WENO algorithm (Jiang & Shu 1996) for baryonic fluid, and N -body simulation for particles of dark matter. The baryon fluid obeys the Navier-Stokes equation, and is gravitationally coupled with collisionless dark matter. We have assumed a standard Λ CDM model, which is specified by the matter density parameter $\Omega_m = 0.27$, baryonic matter density parameter $\Omega_b = 0.044$, cosmological constant $\Omega_\Lambda = 0.73$, Hubble constant $h = 0.71$, the mass fluctuation $\sigma_8 = 0.84$, and scale-free spectrum index $n = 1$. The ratio of specific heats of the IGM is $\gamma = 5/3$. The transfer function is calculated using CMBFAST (Seljak & Zaldarriaga 1996).

The simulation was performed in a periodic, cubic box of size $50 h^{-1}\text{Mpc}$ with a 512^3 grid and an equal number of dark matter particles. It starts at redshift $z = 99$. A uniform UV-background of ionizing photons is switched on at $z = 6$ to heat the gas and reionize the universe. To mimic the enhancement of temperature due to radiation transfer effects (Abel & Haehnelt 1999), a thermal energy of gas with $T = 2 \times 10^4 \text{ K}$ is added in the total energy

at $z = 6$. The clumpy universe would reprocess the photon spectrum from ionizing sources. The reprocessing UV spectrum has been calculated by Haardt & Madau (1996). We use an ionizing background model including QSOs and galaxies with 10% ionizing photons escape fraction (kindly provided by F. Haardt). At $z = 2.5$, such an ionizing background produces the transmission flux of H I and He II similar to observation and an average $\eta \simeq 72$, which is very close to observed value.

The atomic processes in the plasma of hydrogen and helium of primordial composition, including ionization, radiative cooling and heating, and the fraction of H I and He II are calculated in the same way as Theuns et al. (1998). That is, under the “optically thin” approximation, once density and temperature of baryon gas are given, the ionizing state of H and He is directly determined from the ionization-equilibrium equation.

3.2. Samples of Ly α transmitted flux

For given sample of the fields of density, temperature and velocity of the baryon matter, the optical depth of H I or He II can be produced by a convolution with Voigt profile as follows (Bi et al. 1995; Zhang et al. 1997)

$$\tau_i(z) = \sigma_i c \int dx n_i(x) \frac{1}{\sqrt{\pi} H(z) b_i^T} V \left[\frac{\delta z}{b_i^T (1+z)} + \frac{v(x)}{b_i^T}, b_i^T \right] \quad (1)$$

where $i = \text{H I or He II}$, σ_i is the absorption cross section of Ly α line, $n_i(x)$ the number density, δz is the redshift difference between z and x , $v(x)$ the peculiar velocity in unit c and $b_i^T = (2kT/m_i c^2)^{1/2}$ the thermal velocity. V is the Voigt profile, which is normalized $\int dx (1/\sqrt{\pi} b) V \left[\frac{\delta z}{b(1+z)} + \frac{v(x)}{b}, b \right] = 1$. The Hubble constant at redshift z is $H(z) = H_0 \sqrt{\Omega_m (1+z)^3 + \Omega_\Lambda}$. Eq.(1) shows, when the terms of thermal broadening and peculiar velocity are not negligible, the Ly α transmission flux depends on mass density field n_{HI} , n_{HeII} as well as the fields of temperature and velocity of IGM.

We produced 100 mock samples of H I and He II Ly α transmitted flux at $z = 2.5$ with randomly selected lines of sight. Each mock spectrum is sampled using 2^{10} pixels with the same spectral resolution as the observation. As the corresponding comoving scale for 2^{10} pixels is larger than the simulation box size, we replicate the sample periodically. We add Gaussian noise to H I sample with signal-to-noise ratio, S/N=50, while He II with S/N=3. Figure 1 shows typical samples of H I and He II Ly α transmitted flux fields.

4. Line width of He II and H I Ly α absorptions

To demonstrate the importance of the velocity field, we consider the line widths of Ly α absorption. If the Ly α absorption lines are purely thermal broadened, the line width, or Doppler parameter, $b(\text{He II})$ of He II should be less than $b(\text{H I})$ by a factor of 2. However, Zheng et al. (2004) found $b(\text{He II}) = \xi b(\text{H I})$ and $\xi \simeq 1$. They concluded that the velocity field in IGM is dominated by turbulence.

This result can be explained with considering the velocity field in eq.(1). A flux field given by eq.(1) generally is not given by a superposition of lines with Gaussian profile, because the peculiar velocity $v(x)$ is a random field. Therefore, the line width given by Gaussian profile fitting is not always equal to the thermal broadening b^T . For instance, when b_i^T is small, the Voigt profile will picks up only pixels with $\delta z + (1+z)v(x) \simeq 0$. In this case, the line width can be estimated by $(1+z)\langle(\Delta v)^2\rangle^{1/2}$, i.e. the line width is dominated by the variance of the velocity field, which is the same for He II and H I. This is turbulent broadening. It has been shown recently that the velocity field $v(x)$ shows the feature of a fully developed turbulence (He et al. 2006).

To test this point, we identify the absorption lines by the similar way as that for the real sample. We use AUTOVP code (Davé et al. 1997) to decompose the transmitted flux with Gaussian profile, and estimate the parameters of line width, column density, and the centroid wavelength of each line. Figure 2 shows $b(\text{H I})$ vs. $b(\text{He II})$ for both real data and simulation samples. The real data are taken from Zheng et al. (2004). Obviously, the plot of $b(\text{H I})$ vs. $b(\text{He II})$ from simulated data does not follow the thermal broadening relation $b(\text{H I}) = 2b(\text{He II})$, but similar to the turbulent broadening.

5. The ratio between He II and H I Ly α optical depths

5.1. The scatter of optical depth ratio

If the Voigt profile can be approximated by a Dirac delta function, eq.(1) yields

$$\frac{\tau_{\text{HeII}}(z)}{\tau_{\text{HI}}(z)} = \frac{1}{4} \frac{n_{\text{HeII}}(z)}{n_{\text{HI}}(z)}, \quad (2)$$

If atoms and ions of H I, H II, He I, He II and He III are in state of photoionization equilibrium, the ratio of He II to H I is (Fardal et al. 1998)

$$\frac{n_{\text{HeII}}(z)}{n_{\text{HI}}(z)} \simeq 1.70 \frac{J_{\text{HI}}}{J_{\text{HeII}}} \frac{3 + \alpha_4}{3 + \alpha_1} \left(\frac{T(z)}{10^{4.3}} \right)^{0.06}, \quad (3)$$

where we assume that the UV radiation backgrounds around wavelengths wavelength $c/\nu_{\text{HI}} = 912\text{\AA}$ and $c/\nu_{\text{HeII}} = 228\text{\AA}$ are, respectively, $J_\nu = J_{\text{HI}}(\nu/\nu_{\text{HI}})^{-\alpha_1}$ and $J_\nu = J_{\text{HeII}}(\nu/\nu_{\text{HeII}})^{-\alpha_4}$, the parameters J_{HI} and J_{HeII} being the specific intensities, α_1 and α_4 the index of their power laws.

If the UV radiation background is spatially uniform, i.e. the parameters J_{HI} , J_{HeII} , α_1 and α_4 are constant, the ratio $n_{\text{HeII}}(z)/n_{\text{HI}}(z)$ of eq.(3) is approximately spatially constant, because the temperature-dependence ($T^{0.06}$) is very weak. Thus, from eqs.(2) and (3) we may expect that the ratio of optical depths $\tau_{\text{HeII}}(z)/\tau_{\text{HI}}(z)$ should basically be constant, i.e. the scatter of ratio $\tau_{\text{HeII}}(z)/\tau_{\text{HI}}(z)$ with respect to its mean $\langle \tau_{\text{HeII}}(z)/\tau_{\text{HI}}(z) \rangle$ has to be very small.

Thus, the observed η scatter (Kriss et al. 2001; Smette et al. 2002; Zheng et al. 2004; Shull et al. 2004) may indicate that the ratios, $J_{\text{HI}}/J_{\text{HeII}}$ and $(3 + \alpha_4)/(3 + \alpha_1)$ are not constant, but significantly different from pixel to pixel, or from line to line. However, eq.(2) is based on the assumption that the effects of thermal broadening and peculiar velocities are ignored. As has been shown in last section, the effects of thermal broadening and peculiar velocities may not be always small. Therefore, we should estimate the η -scatter caused by thermal broadening and peculiar velocities.

Since the assumption of eq.(2) is not hold, we use η to stand only for $4\tau_{\text{HeII}}/\tau_{\text{HI}}(z)$ below. Figure 3 illustrates the effect of thermal broadening and a peculiar velocity field. It shows 1.) top panel: the 1-D distributions of the ratio η of optical depths given by eq.(1), 2.) second panel: η distribution from optical depths of eq.(1), but using a delta function for the Voigt profile; 3.) third panel: η given by optical depths of eq.(1) and adding, respectively, $S/N=3$ and $S/N=50$ noises to the He II and H I transmitted flux; 4.) forth panel: temperature T distribution; 5.) bottom panel: mass density field of baryon matter.

From the panel 2 of Fig. 3 one can see clearly that if the effect of thermal broadening is ignored, i.e. the Voigt profile is approximated by a Dirac delta function, η is almost a constant in the whole range. In this approximation, the ratio η does not depend on the fluctuations of temperature, mass density and velocity of baryon gas, but only on the density ratio $n_{\text{HII}}/n_{\text{HI}}$. The ratio $n_{\text{HII}}/n_{\text{HI}}$, however, always keeps constant, even when n_{HII} and n_{HI} fluctuate strongly. The η distribution shown in panel 2 contains a significant sharp decline at the highest temperature region. It probably results from dielectronic recombination of He II that is dominant at such high temperatures, and reduces the number n_{HeII} . At less high temperatures, the collision ionization rate of H I is higher than He II, accordingly, there appear some small bumps as those visualized in panel 2.

However, the top panel shows that, when thermal broadening is included, the fluctu-

ations of η are higher at the positions with higher temperature and higher density. These fluctuations are due partially to the difference between the thermal velocities of He II and H I. It leads to the distribution of H I to be more extended than He II. The hydrodynamical velocity field $v(x)$ is the same for He II and H I. It doesn't cause the change of the ratio $n_{\text{HII}}/n_{\text{HI}}$. The effect of thermal broadening on η scatter has also been noted by Croft et al. (1997), but in their samples the scatter caused by thermal broadening is not very significant. It is probably because more shocks are resolved on small scales in the WIGEON simulations, which leads to stronger temperature fluctuations (He et al. 2004). The panel 3 of Fig. 3 shows more significant scatter of η if the noise is added. From Figure 1, we have seen that the transmitted flux of He II is substantially affected by the S/N=3 noise.

5.2. PDF of η

We now examine the probability distribution function (PDF) of η , which is calculated pixel by pixel as Shull et al. (2004). Figure 4 shows the PDFs for 1.) real data; 2.) simulation sample of the transmitted flux from eq.(1); 3.) simulation samples of the transmitted flux from eq.(1), and adding, respectively, S/N=3 and S/N=50 noise to the He II and H I transmitted flux, and 4.) simulated samples without thermal broadening, but adding noise. The simulation PDFs are calculated with 100 samples of 1-D transmitted flux of He II and H I. The error bars are the maximum and minimum from 100 independent noise realizations. The simulation data are also binned into 0.05Å to match observation.

We see that the PDF of the simulated data without adding noise has the peak at $\log \eta \simeq 1.9$ which is about the same as real data (Zheng et al. 2004; Shull et al. 2004). However, the width of PDF of the simulated data without adding noise is much less than the real data. The maximum scatter of η of the simulated data is about $2\langle\eta\rangle$. The factor 2 is just the difference between the thermal velocities of H I and He II. Though there are some pixels with $\eta > 2\langle\eta\rangle$ caused by collision ionization, it is still less than the observed scatter.

The PDF of simulation data is significantly improved with adding noise. It looks similar to the observed result. The PDF of simulation data has the same peak as real data, and the width of PDF is also about the same as real one. Therefore, the effect of data noise is substantial for the scatter of η . This effect is especially serious on the high η events. Samples without noise contamination do not have events of $\eta > 300$, but the samples with noise do. This result is about the same as Shull et al. (2004), in which events of $\eta > 460$ are dropped, because they may largely be from the uncertainty in measuring.

Nevertheless, we see that the PDF of simulation sample with noise is still lower than

the real data in the range $\eta < 10$. This result is also similar to Shull et al. (2004). They found that the events of $\eta < 10$ of real data show an factor 2 excess to a Monte Carlo calculation. Figure 4 also shows that the number of $\eta < 10$ of real data is about twice as large as simulation sample. However, Shull et al. (2004) found that the events of $\eta < 30$ of real data are also more than their Monte Carlo estimation by a factor 2, while Figure 3 doesn't show so large difference. This is probably because our simulation contains the effect of thermal broadening and peculiar velocity field. This point can be seen from the PDF of η for simulation samples without thermal broadening, but adding noise (the filled dots in Figure 4). It shows there are more low- η events without thermal broadening. In a word, our simulation result indicates the excess of low- η events in real data, but the difference between real and simulation data is less than the Monte Carlo estimation.

The effect of noise can also be seen in Figure 5, which presents the relation between η and τ_{HI} in the range $\tau_{\text{HI}} > 0.01$. The top panel is from real data. The middle is given by simulation samples with adding noise of S/N=3 to He II and S/N=50 to H I. The bottom shows simulation samples without noise. The η - τ_{HI} distribution of simulation sample with noise is similar to the real one. The high- η events at low τ_{HI} area are mainly from noise. This is consistent with the observed result that η is large in void area $\tau_{\text{HI}} < 0.05$ (Shull et al. 2004).

Figure 6 presents the relation between η and column density $N(\text{HI})$ for real data and simulation samples with noise. It shows the correlation between η and density of H I: η is larger for lower column density $N(\text{HI})$, and lower for higher $N(\text{HI})$. This phenomenon is also shown in the He II spectrum of HS1700+6416 (Reimers et al. 2005).

6. Power spectrum

We now compare the power spectra of H and He transmitted flux of simulation sample and real data. We calculate the power spectrum by the same method as Paper I. It gives easy to compare the power spectra of H and He. Moreover, the real data of He is highly noisy, for some pixels, the S/N ratio is lower than 1, and some pixels with negative flux. To eliminate the effect of these pixels on the power spectrum calculation, we should use the algorithm of denoising or conditional-counting as Paper I (Donoho 1995; Jamkhedkar et al. 2001).

The power spectra of H I and He II Ly α transmitted flux of HE2347 are shown in Figure 7. We plot the power spectrum of H I in top panel as an indicator of the goodness of the simulation sample of this paper, which is produced in a box with size larger than that of

Paper I by a factor of 4. The parameters $f = 1$ and $f = 3$ mean, respectively, the threshold condition for denoising to be $S/N > 1$, and 3. Since the real data of H I Ly α transmitted flux has high quality, the power spectrum actually is f -independent if $f > 1$ (Jamkhedkar et al. 2005). On the other hand, there are very rare pixels of the He II data with $S/N > 3$, and therefore, only a very small number of the modes is available if taking $f > 3$. One can only use $f = 1$ to calculate He II power spectrum of HE2347. The error bars of Figure 7 is estimated by the maximum and minimum range of bootstrap re-sampling.

As expected, the simulation sample of H I transmission flux is in well agreement with observations on all scales less than $\delta v = 224 \text{ km s}^{-1}$. There is no discrepancy on the smallest scale $\delta v = 28 \text{ km s}^{-1}$ or length scale $D = 0.28 \text{ h}^{-1} \text{ Mpc}$. This result is the same as Paper I, and therefore, the power spectrum on small scales is insensitive to the size of simulation box.

The power spectrum of the He II Ly α transmitted flux of HE2347, as shown in the bottom panel of Figure 7, is very different from simulation samples without adding noise on scales less than 56 km s^{-1} . On those scales, the power spectrum of observed sample is much higher than the simulation results. However, the power spectrum of the noisy samples of He II flux gives a good fitting to the observed sample. In other words, if we could remove the $S/N=3$ noise from the real data, the power spectrum can be well fitted with the simulation of the Λ CDM model. Thus, with He II flux, we can arrive at the same conclusion as H I: there is no evidence for the discrepancy between observation and simulation on scales from 1792 to 28 km s^{-1} , or from 0.28 to $18 \text{ h}^{-1} \text{ Mpc}$.

7. Discussions and conclusions

The H I and He II Ly α transmitted flux fluctuations of QSO absorption spectrum are valuable to detect the fields of baryon gas and ionizing photon field, and to constrain models of the UV radiation background. With hydrodynamic simulation samples of the Λ CDM model, we made a comparison between the model-predicted statistical features and real data of HE2347. It includes the power spectrum, the line width of absorption features, and the ratio between the He II and H I optical depths. The major conclusions are as follows:

1.) The absorption features of He II and H I basically are turbulent-broadening. It should be emphasized that the observed evidence for the turbulent-broadening mainly is given by the absorption lines in voids (Zheng et al. 2004). This is especially supported by the simulation samples, which shows that the turbulence behavior of the velocity field of IGM is on high as well as low mass density area (Kim et al. 2005).

2.) The mean of the optical depth ratio $\langle \eta \rangle$ of real sample can be well fitted with simulation samples.

3.) The simulation samples give a very well fitting to the power spectra of both H I and He II transmitted flux. There is no discrepancy between the power spectra of simulated and observed samples on small scales. For H sample, the scales are till to $0.28 \text{ h}^{-1} \text{ Mpc}$. For He, it is $1.1 \text{ h}^{-1} \text{ Mpc}$. Therefore, there is no evidence that the power of observed sample is less than the standard ΛCDM model on small scales.

4.) The last but not the least is on the η -scatter. The large η scatter are generally attributed to the inhomogeneity of the UV photon distributions. We showed, however, that a significant part of the η -scatter is from the fluctuations of the temperature and velocity fields of IGM and data noise. There seems to be a discrepancy on low- η events comparing our simulation and the real data. The simulation sample does not contain enough low- η events to fit real data. To solve this problem models of producing extra fluctuations on Ly α transmitted flux on scales of about $1 \text{ h}^{-1} \text{ Mpc}$ is needed.

The WIGEON samples are produced with a uniformly distributed UV radiation background, and therefore, we may consider an inhomogeneous UV radiation background to be a possible reason of the lack of low- η events. However, the numerical results of the inhomogeneous UV radiation background shows that the fluctuations of UV radiation background on small scales will yield more high- η events ($200 < \eta < 350$). Therefore, at least, according to the current calculation, the model of the UV background inhomogeneity would not be helpful to solve the problem of the lack of low- η events.

Note that low- η events are related to high column density $N(\text{HI})$. The lack of low- η events may be due to that the WIGEON samples are produced without considering the detailed physical processes of ionizing sources, as some mechanical and radiation feedback effects would not be negligible in the area of high column density, which has the high probability containing collapsed objects.

Any model of producing the scatter of η will affect the transmitted flux of both H I and He II. Therefore, we can use our unified fitting of H I and He II Ly α transmitted flux to set some constraints on models for low- η events.

First, if the fluctuations are Gaussian, it will play the same role as Gaussian noise, and increase the power of transmitted flux on scale $\simeq 1 \text{ Mpc}$. However, this paper and Paper I show that the power spectrum of H I Ly α transmitted flux is in good consistent with observation on scale $1 \text{ h}^{-1} \text{ Mpc}$ and less. Therefore, any increase of the power of simulation sample will no longer be consistent with observed sample. Therefore, there is small room for models of adding Gaussian fluctuation.

Second, if the fluctuations are non-Gaussian, it should be limited by the observed non-Gaussian features of the H I and He II flux. The non-Gaussian statistical features of H I transmitted flux, such as high order moments of the fluctuations of the flux, are sensitive to the addition of non-Gaussian inhomogeneity. It has been shown in Paper I that the non-Gaussian features of the H I transmitted flux of HE2347 can already be well fitted with the WIGEON samples to eight order and on scale as small as $0.28 \text{ h}^{-1} \text{ Mpc}$. Therefore, there is also small room for models of adding non-Gaussian fluctuations.

JRL thanks Francesco Haardt for kindly providing us ionizing background model, Romeel Davé for making AUTOVP publicly available and Hy Trac for help from his MACH code. We thank our referee for helpful suggestions on shaping our paper. LLF acknowledges support from the National Science Foundation of China (NSFC). This work is partially supported by the NSF AST-0507340.

REFERENCES

Abel, T. & Haehnelt, M. G. 1999, ApJ, 520, L13

Bi, H.G., Ge, J., & Fang, L.Z. 1995, ApJ, 452, 90

Boksenberg, A., Sargent, W., & Rauch, M. 2003 astro-ph/0307557

Cen, R., & Ostriker, J. P. 1999, ApJ, 514, 1

Croft, R. A. C., Weinberg, D. H., Katz, N., & Hernquist, L. 1997, ApJ, 488, 532

Daubechies I. 1992, *Ten Lectures on Wavelets* (Philadelphia: SIAM)

Davé, R., Hernquist, L., Weinberg, D. H., & Katz, N. 1997, ApJ, 477, 21

Davé, R., et al. 2001, ApJ, 552, 473

Donoho, D.L. 1995, IEEE Transactions on Information Theory, 41, 613

Fang, L.Z., & Feng, L.L. 2000, ApJ, 539, 5

Fang, L.Z., & Thews, R. 1998, *Wavelet in Physics* (Singapore: World Scientific)

Fardal, M. A., Giroux, M. L., & Shull, J. M. 1998, AJ, 115, 2206

Farge, M., Kevlahan, N., Perrier, V. & Goirand, E. 1996, Proceedings of the IEEE, 84, 639

Feng, L.L., Shu, C.W., & Zhang, M.P. 2004, ApJ, 612, 1

Flores, R., & Primack, J. 1994, ApJ, 427, L1

Haardt, F., & Madau, P. 1996, ApJ, 461, 20

He, P., Feng, L.L., & Fang, L.Z. 2004, ApJ, 612, 14

He, P., Liu, J.R., Feng, L.L., Shu C.-W. & Fang, L.Z. 2006, Phys. Rev. Lett, 69, 051302

Hu, E.M. et al. 1995, AJ, 110, 1526-43

Jamkhedkar, P., Bi, H.G., & Fang, L.Z. 2001, ApJ, 561, 94

Jamkhedkar, P., Feng, L.L., Zheng , W., Tytler, D., Kirkman, D., & Fang, L. Z., 2003, MNRAS, 343, 4

Jamkhedkar, P., Feng, L.L., Zheng , W., & Fang, L. Z., 2005, ApJ, 633, 52 (Paper I)

Jiang, G., & Shu, C.W., 1996, J. Comput. Phys. 126, 202

Kim, B., He, P., Pando, J., Feng, L. L. & Fang, L. Z. 2005, ApJ, 625, 599

Kim, T.S., Viel, M., Haehnelt, M. G., Carswell, R. F., & Cristiani, S. 2004, MNRAS, 347, 355

Kriss, G. A., et al. 2001, Science, 293, 1112

Maselli, A., & Ferrara, A. 2005, MNRAS, 364, 1429

McGaugh, S. S., Barker, M.K., & de Blok, W. J. G. 2003, ApJ, 584 566

Pando, J. & Fang, L.Z., 1998, Phys. Rev. E57, 3593

Reimers, D., et al. 2005, astro-ph/0410588

Seljak, U., & Zaldarriaga, M. 1996, ApJ, 469, 437

Smette, A., et al. 2002, ApJ, 564, 542

Shull, M. I., Tumlinson, J., Giroux, M. L., Kriss, G. A., & Reimers, D. 2004, ApJ, 600, 570

Simon, J. D., Bolatto, A. D., Leroy, A., & Blitz, L. 2003, ApJ, 596, 957

Swaters, R. A., Madore, B. F., van den Bosch, Frank C., & Balcells, M. 2003, ApJ, 583, 732

Theuns, T., Leonard, A., Efstathiou, G., Pearce, F. R., & Thomas, P. A. 1998, MNRAS, 301, 478

Zentner, A. R., & Bullock, J. S. 2003, ApJ, 598, 49

Zhang, Y., Anninos, P., & Norman, M. L. 1995, ApJ, 453, L57

Zhang, Y., Anninos, P., Norman, M. L., & Meiksin, A. 1997, ApJ, 485, 469

Zheng, W., et al., 2004, ApJ, 605, 631

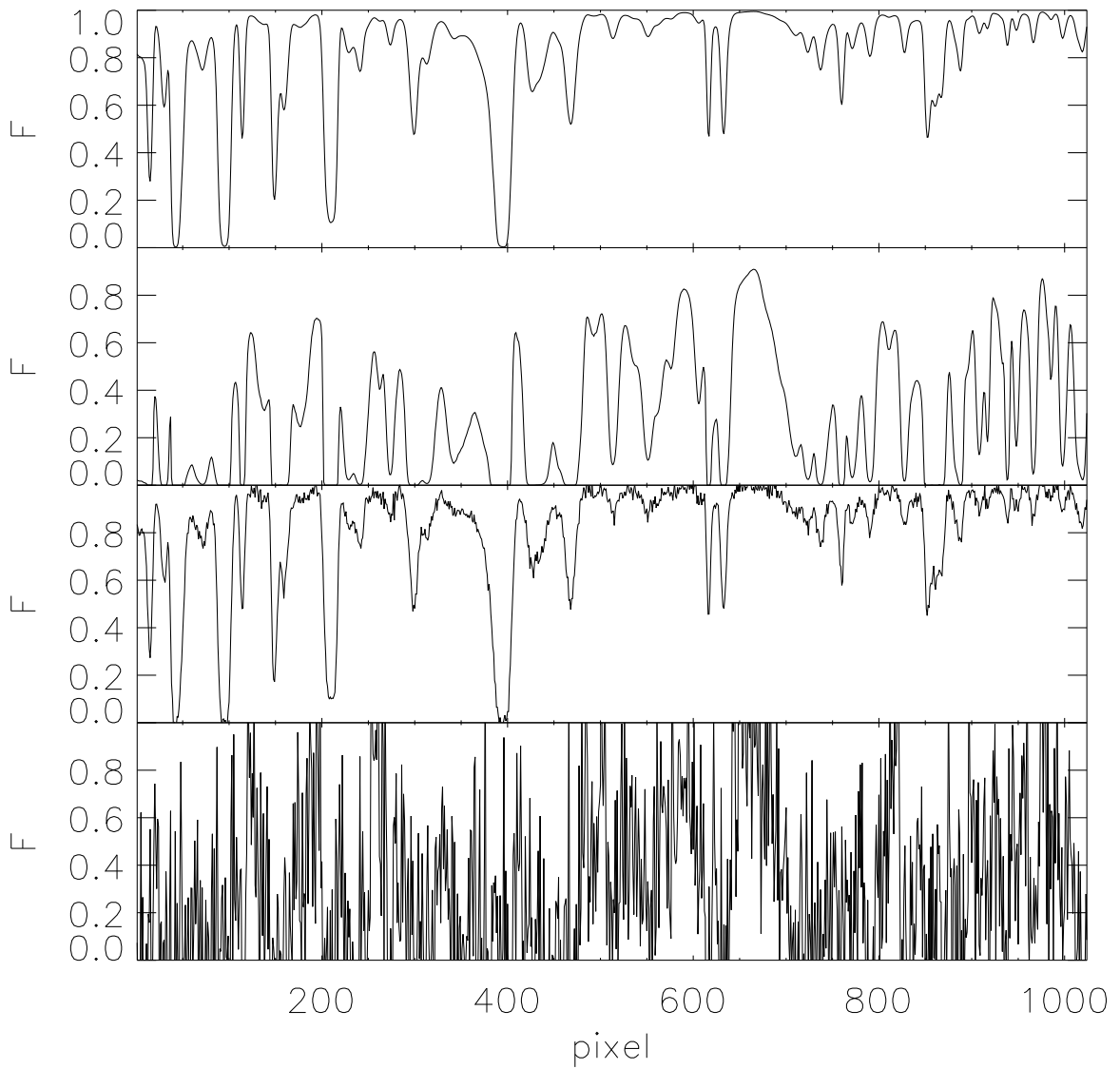


Fig. 1.— Simulated samples of H I (top) and He II (second from top) transmitted flux without adding noise, and the same samples of H I (third from top) and He II (bottom) with adding noise with $S/N=50$ for H I and $S/N=3$ for He II.

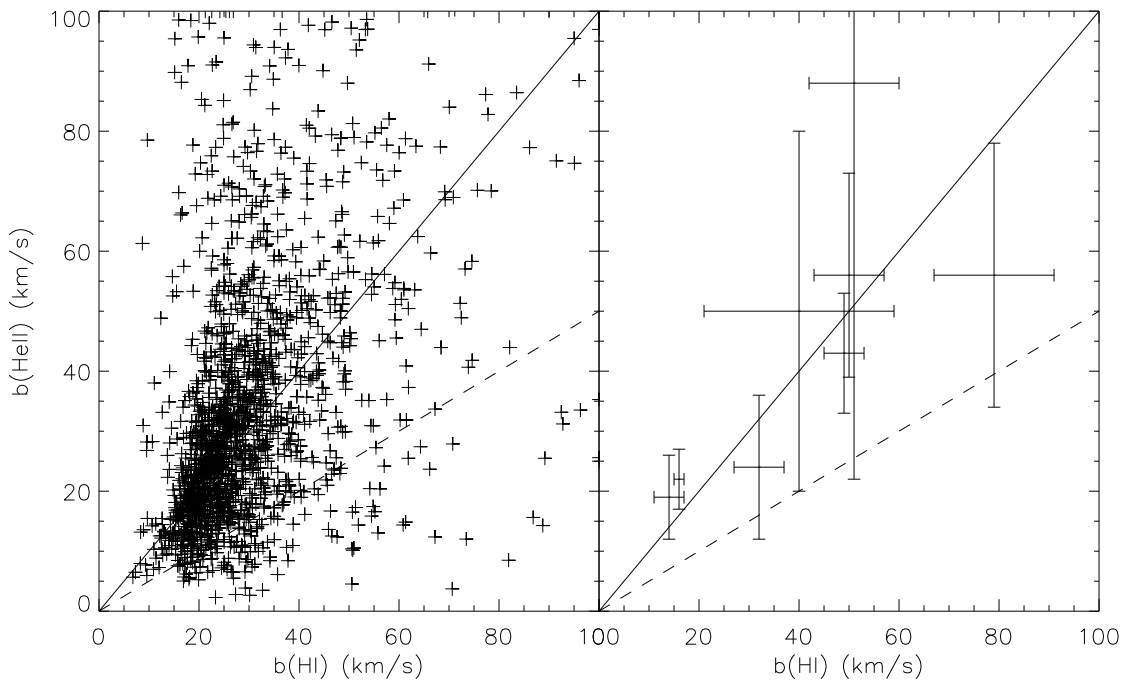


Fig. 2.— Doppler parameter $b(\text{H I})$ vs. $b(\text{He II})$ of simulation samples (left) and real data of HE2347 (right). The diagonal line is expected for turbulent broadening and the dashed line is for $b(\text{H I}) = 2b(\text{He II})$.

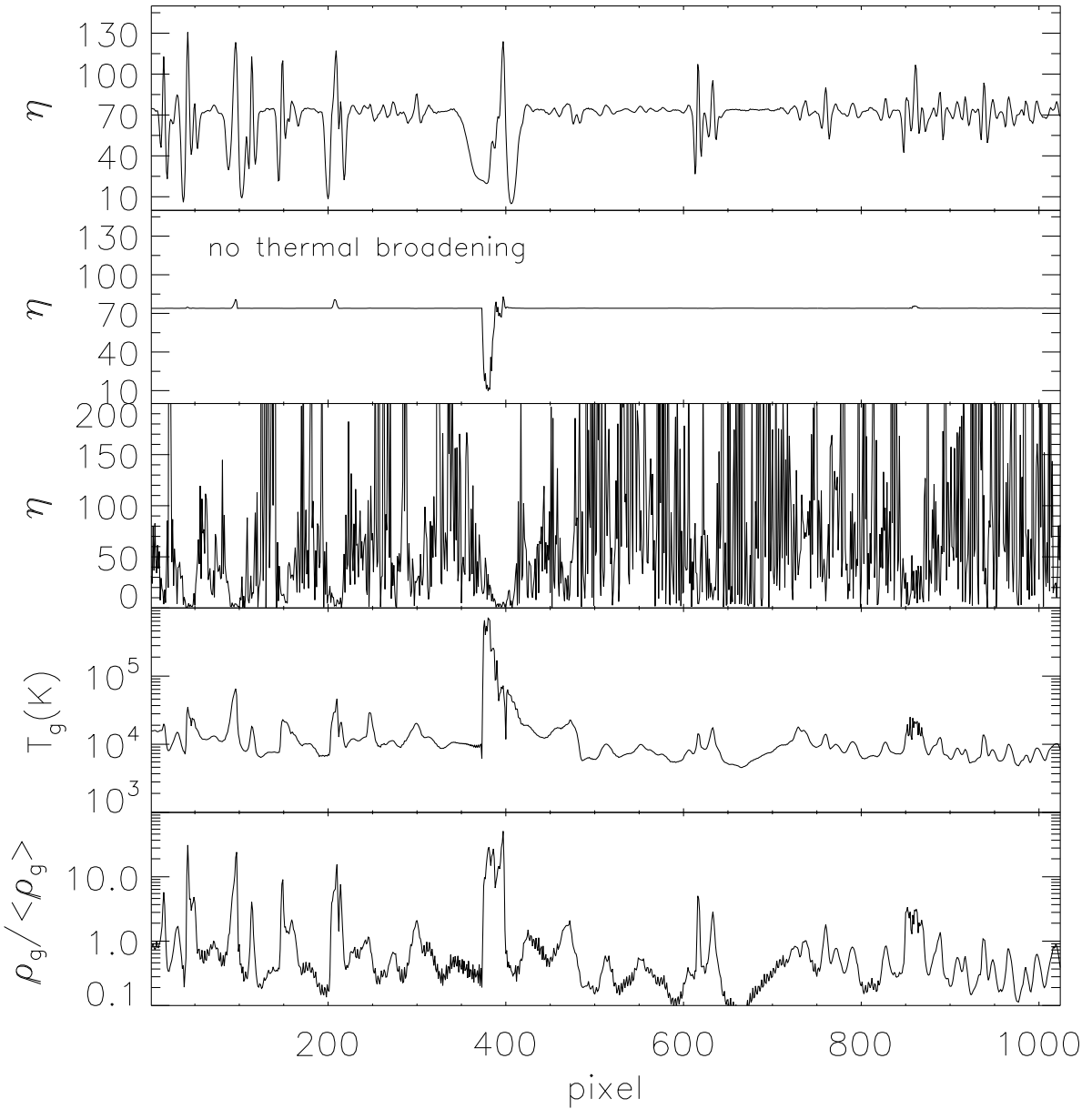


Fig. 3.— 1-D distribution of η with (top) and without (next top) thermal broadening. The third panel shows η with adding S/N= 50 noise to H I and S/N=3 noise to He II flux. The temperature and baryon matter density are also shown.

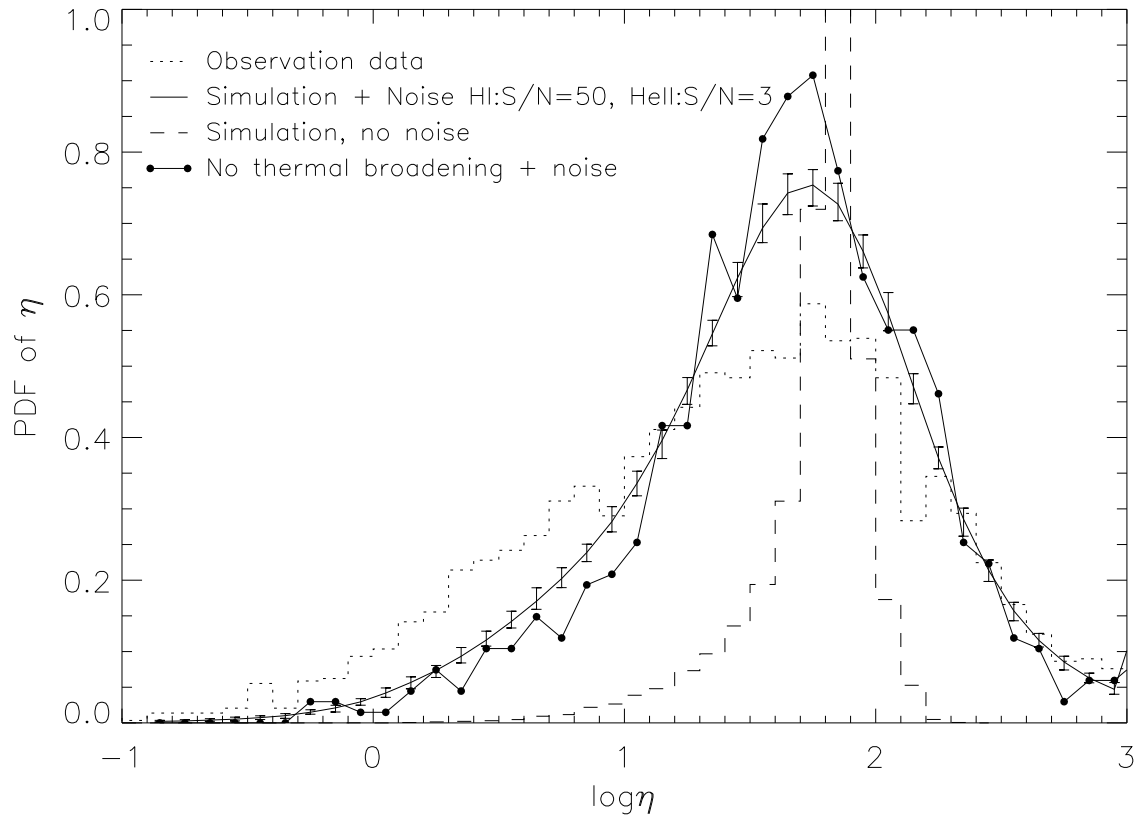


Fig. 4.— PDF of η . 1. Real data (dot line); 2. Simulation samples with adding S/N=50 noise to H I and S/N=3 noise to He II transmitted flux (solid line), errorbars being the maximum and minimum over 100 independent noise realizations; 3. Simulation samples without noise (dashed line); 4. Simulation samples without thermal broadening, but adding noise.

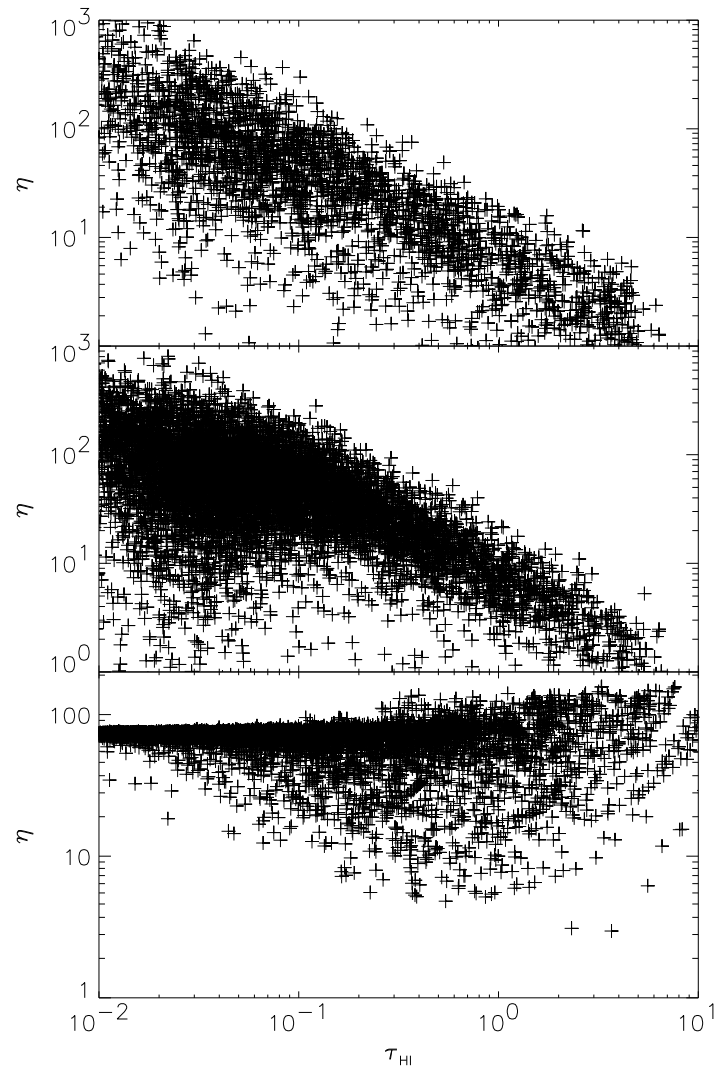


Fig. 5.— η vs. optical depth τ_{HI} for real data (top); simulation samples with noise (middle) and without noise (bottom).

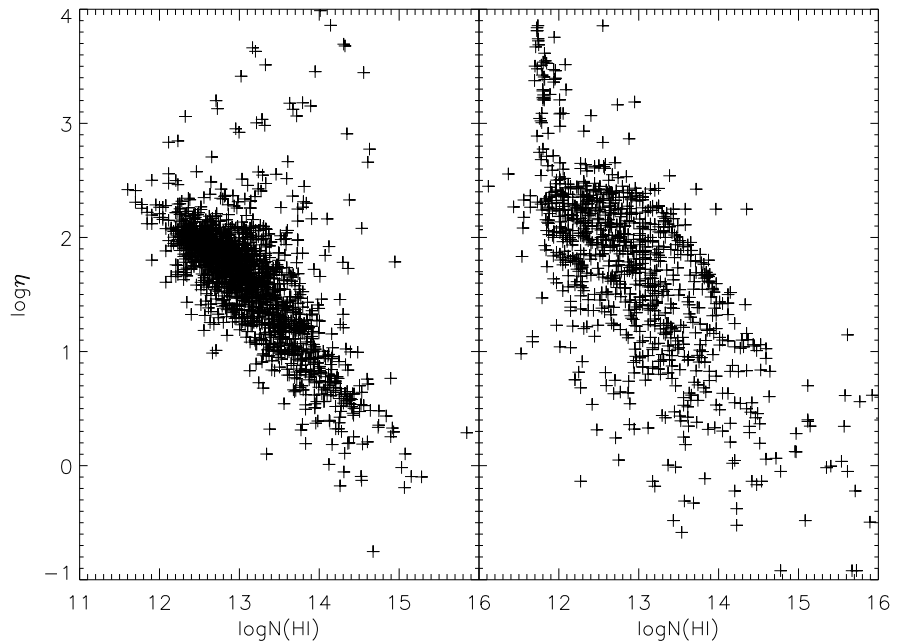


Fig. 6.— η vs. column density $N(\text{HI})$ for simulation data (left) and real data of HE2347 (right).

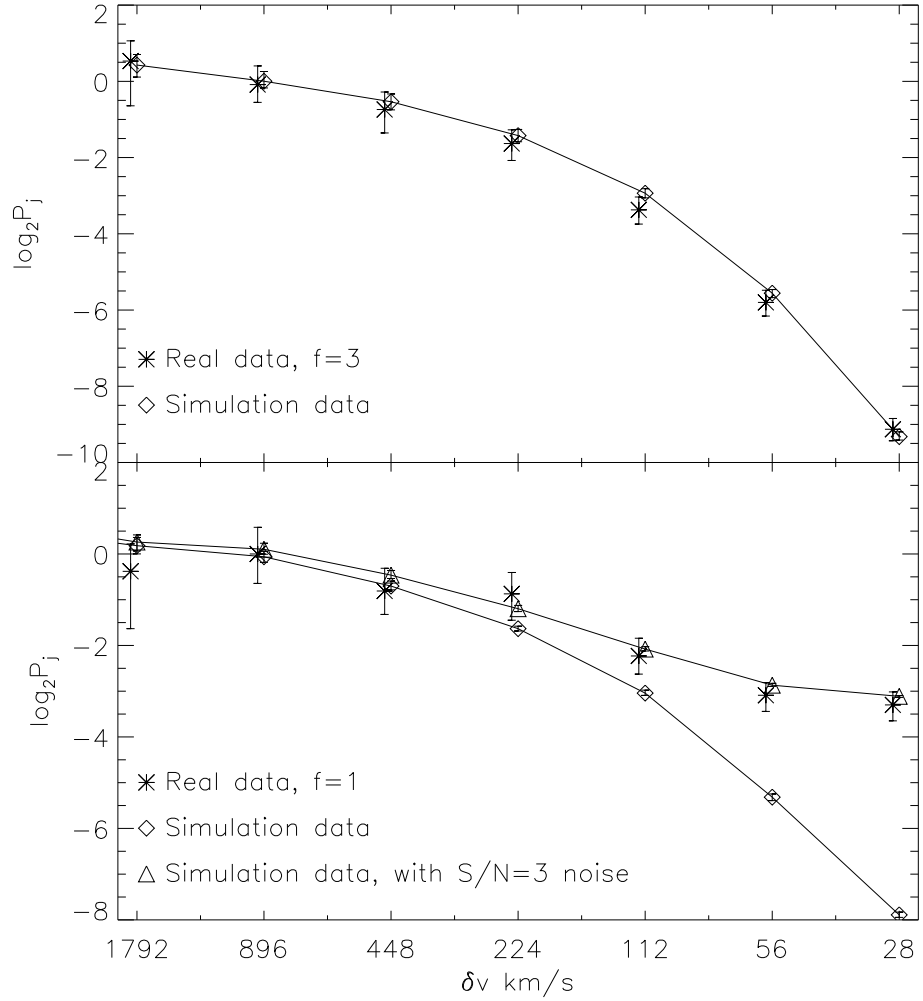


Fig. 7.— Power spectrum of 1.) H I transmitted flux of HE2347 with the conditional counting parameter $f = 3$ for real data (*) and simulation sample (\diamond) (top); 2.) He II transmitted flux of HE2347 with the conditional counting parameter $f = 1$ for real data (*), simulation sample with adding noise of $S/N=3$ (\triangle) and without noise adding (\diamond) (bottom).